

Effect of Ir substitution in the ferromagnetic superconductor
 $\text{RuSr}_2\text{GdCu}_2\text{O}_8$

A. R. Jurelo^{1,*}, S. Andrade¹, R. F. Jardim^{1,†}, F. C. Fonseca²,
M. S. Torikachvili³, A. H. Lacerda⁴, and L. Ben-Dor⁵

¹*Instituto de Física, Universidade de São Paulo,
CP 66318, 05315-970, São Paulo, SP, Brazil*

²*Instituto de Pesquisas Energéticas e Nucleares,
CP 11049, 05422-970, São Paulo, SP, Brazil*

³*Department of Physics, San Diego State University, San Diego, California 92182-1233*

⁴*National High Magnetic Field Laboratory (NHMFL),
Los Alamos National Laboratory, Los Alamos, New Mexico 87545*

⁵*Department of Inorganic and Analytical Chemistry,
Hebrew University, Jerusalem 91904, Israel*

(Dated: October 29, 2018)

Abstract

A detailed study of the effect caused by the partial substitution of Ru by Ir on the magnetic and superconducting properties of the ruthenocuprate $\text{Ru}_{1-x}\text{Ir}_x\text{Sr}_2\text{GdCu}_2\text{O}_8$; $0 \leq x \leq 0.10$; is presented. The combined experimental results of structural, electrical, and magnetic measurements indicate that Ir substitutes Ru for $x \leq 0.10$ with no significant structural distortions. Ir-doping gradually suppresses both the magnetic and the superconducting states. However, all samples were observed to attain the zero-resistance state at temperatures ≥ 2 K up to the highest applied magnetic field of 18 T. The resistive upper-critical field H_{c2} as a function of temperature has been determined for these polycrystalline samples. Values of $H_{c2}(0)$ were found to be ~ 52 T, and weakly dependent on the Ir concentration. We have also observed that the superconducting transition width decreases and the slope of the resistive transition increases with increasing Ir doping, a feature which is much more pronounced at high applied magnetic fields. The double-peak structure observed in the derivative of the resistive curves has been related to an inhomogeneous nature of the physical grains which is enhanced due to the Ru substitution by Ir. This indicates that the Josephson-junction-array (JJA) model seems to be appropriated to describe the superconducting state in these ruthenocuprates. The low temperature $\rho(T)$ data along with the determined vortex thermal activation energy are consistent with a 2D vortex dynamics in these materials.

PACS numbers: 74.25.Ha, 74.62.-c, 74.72.-h

Keywords: magnetic superconductors, rutheno-cuprate superconductor, high- T_c

I. INTRODUCTION

The study of the coexistence of superconductivity and magnetic ordering in the ruthenocuprate $\text{RuSr}_2\text{GdCu}_2\text{O}_8$ (Ru-1212) has attracted great interest since the original study of Bauernfeind *et al.*¹ The Ru-1212 is a 1212-type layered cuprate structurally similar to the $\text{YBa}_2\text{Cu}_3\text{O}_{7-\delta}$ (YBCO), where Y and Ba are replaced by Gd (or Eu) and Sr, respectively, and the Cu-O chains replaced by RuO_2 layers.^{1,2} In these materials the magnetic long-range ordering of the Ru sub-lattice occurs below a transition temperature $T_M \sim 130$ K while the superconductivity arising from the CuO_2 layers occurs below a critical temperature $T_c \sim 40$ K. Recent studies have indicated that the magnetic ordering and the superconducting state are essentially decoupled, being related only by the charge transfer between Ru and CuO planes.³ In addition to this, there is no clear evidence about the exact nature of the magnetic structure of these materials up to now but it is accepted that, for low magnetic fields, there is an antiferromagnetic (AFI) order, whereas for high magnetic fields ($H \sim 2$ T) a spin-flop transition is observed,⁴ with Ru magnetic order essentially ferromagnetic (FM). Also, from experimental data and theoretical analysis, it was proposed that for temperatures lower than T_c , the magnetic-flux lines are present even without an external magnetic field, suggesting the creation of a spontaneous vortex phase (SVP).^{5,6}

In fact, the genuine coexistence of superconductivity and magnetism at microscopic level is still controversial. Some experimental studies⁷ have shown that the ruthenocuprates are microscopically uniform. On the other hand, several experimental results have indicated a possible phase-separation of superconducting (SC) and magnetic regions.^{8,9,10} For instance, high-resolution transmission electron microscopy (HRTEM) and synchrotron X-ray diffraction analysis have suggested a phase separation in Ru-1212 compounds.⁸ It was argued that such a phase separation arises from the rotation of the RuO_6 octahedra around the c -axis, resulting in the formation of small domains with characteristic lengths ≤ 200 Å separated by sharp antiphase boundaries of reversed rotations.⁸ Also, a phase separation between FM and AFM nanodomains inside physical grains of Ru-1212 has been proposed from a detailed analysis of magnetization data.^{9,10} The authors have concluded that intragrain properties of the ruthenocuprates exhibit features of granular superconductors and a Josephson-junction-array (JJA) model was invoked to account for the intrinsic inhomogeneities of intragrain superconductivity.^{9,10} Therefore, a discussion of whether both superconducting and mag-

netic phases originate from the same crystallographic structure, and features of this intimate coexistence on a microscopic scale are relevant questions for the understanding of these materials.

Considering that the coupling allowing for the coexistence of superconductivity and ferromagnetism in Ru-1212 compounds is very weak and strongly affected by chemical substitutions, the dilution of the magnetic Ru sublattice by different ions is an interesting approach to probe the coexistent phenomena. The partial substitution of Ru by Sn^{4+} was found to suppress the FM moment of the sublattice and to increase the onset of the SC transition. These features would reflect an increase in the transfer rate of holes to the CuO_2 planes.¹¹ Studies regarding substitution of Ru by both Ti and Rh revealed that both FM and SC transition temperatures are reduced upon increasing dopant concentration.¹² The substitution of Ru by Nb^{5+} results in a decrease of the magnetic ordering temperature and an increase in the Ru valence,¹³ whereas for Ta-substituted specimens an apparent suppression of the superconductivity of Ru-1212 has been observed.¹⁴ In general, both magnetic and superconducting properties of the ruthenocuprates are affected by the ionic radius, valence, and magnetic character of the substituting ion. However, changes observed in alloying Ru-1212 compounds are usually accompanied by significant structural distortions due to differences in ionic radii. Within this scenario it is a difficult task to distinguish between changes arising from properties of the substituted ion and those from crystallographic distortions.

In the present work we have investigated the crystallographic, transport, and magneto-transport properties of $\text{Ru}_{1-x}\text{Ir}_x\text{Sr}_2\text{Gd}_1\text{Cu}_2\text{O}_8$ compound in order to study the relationship between superconductivity and magnetism. We have found that Ir substitutes Ru up to 10 % in Ru-1212 without appreciable structural changes. In addition to this, the combined data indicate a possible phase-separation in the Ru-1212 compound.

II. EXPERIMENTAL PROCEDURE

Polycrystalline samples of $\text{Ru}_{1-x}\text{Ir}_x\text{Sr}_2\text{GdCu}_2\text{O}_8$ (Ru(Ir)-1212); $0 \leq x \leq 0.10$; were prepared following a two-step procedure.¹⁵ The two-step synthesis minimizes the formation of the SrRuO_3 phase, yielding samples with better quality.¹⁶ Initially, the $\text{Sr}_2\text{GdRu}_{1-x}\text{Ir}_x\text{O}_6$ (Sr-2116) precursor was prepared by mixing stoichiometric quantities of high purity Ru, Ir, SrCO_3 , and Gd_2O_3 , grinding together and heating in air at 1250 °C for 12 h. Then, CuO was

mixed to the Sr-2116 powders, ground together, pressed into pellets, and sintered at 1060 °C for 72 hours in flowing O₂. The crystal structure of the samples was analyzed by X-ray powder diffraction (XRD) measurements using CuK_α radiation on a Bruker D8 Advance diffractometer. The diffraction patterns were collected in the 2Θ range 20° to 80° with a step of 0.01 and 8 s counting time. Rietveld refinements of crystal structures were performed using the GSAS software. The temperature dependence of the magnetoresistance $\rho(H, T)$ was measured by the standard four-probe method using a Linear Research Model LR-700 bridge operating at 16 Hz. In all transport measurements, copper electrical leads attached to Ag film contact pads (made with Ag epoxy) on parallelepiped-shaped samples with typical dimensions of 5 x 2 x 1.5 mm³. The magnetoresistance experiments were performed at the National High Magnetic Field Laboratory, Los Alamos, in the temperature range from 2 to 300 K and under magnetic fields H up to 18 T. Measurements at low applied magnetic fields H up to 0.5 T were performed in a home-made apparatus using a superconducting coil with very low remnant field. The samples were characterized by both magnetization $M(T)$ and ac magnetic susceptibility $\chi_{ac}(T)$ using a SQUID magnetometer from Quantum Design. Magnetization measurements in the remnant field (~ 1 Oe) of the superconducting magnet were performed in the temperature range from 5 to 300 K in both zero-field-cooled (ZFC) and field-cooled (FC) modes. The T-dependence of the ac magnetic susceptibility (f = 155 Hz) was measured with an excitation field of 2 Oe.

III. RESULTS AND DISCUSSION

The X-ray diffraction patterns of Ru_{1-x}Ir_xSr₂GdCu₂O₈ (Ru(Ir)-1212) for $x = 0.00$ and $x = 0.10$ are displayed in Fig. 1. All the samples were found to be nearly single-phase although small fractions of SrRuO₃ and Sr-2116 (≤ 2 %) could be detected. The volume fraction of the extra phases were found to show no dependence on the Ir concentration. The diffraction peaks of the desired phase were indexed as belonging to the Ru-1212 tetragonal phase, space group $P4/mmm$. The inset of Fig. 1 shows the calculated lattice parameters as a function of the Ir content in this series. The refined lattice parameters of the pristine compound $a = b = 3.8389(1)$ Å, and $c = 11.5652(1)$ Å are close to the values reported previously.⁸ The six-fold coordination of Ir⁵⁺ and Ir⁴⁺ have ionic radii values very close to Ru⁵⁺ and Ru⁴⁺,¹⁷ respectively, and the lattice parameters yielded by the Rietveld analysis

are essentially Ir content independent, as displayed in Fig. 1. In addition, the Rietveld refinement for the specimen with Ir $x = 0.10$ doesn't show an orthorhombic distortion, which further suggests that the space group $P4/mmm$ is preserved for the range of Ir content here investigated.⁸ This assumption is supported by recent results where the Ir-1212 phase has been successfully synthesized and found to exhibit a tetragonal crystal structure, space group $P4/mmm$.¹⁸ These results indicate that Ir substitutes Ru in this series. The crystallographic parameters for the samples with $x = 0.00$ and 0.10 specimens obtained by the refinements are summarized in Table I.

Figure 2 shows the temperature dependence of the electrical resistivity of Ru(Ir)-1212 at zero external magnetic field. The measured $\rho(T)$ are within the range of the reported values for the Ru-1212 compound and, upon Ir doping the resistivity at room temperature increases from $\rho(300\text{ K}) \sim 15\text{ m}\Omega\text{cm}$ to $\sim 21\text{ m}\Omega\text{cm}$ for $x = 0.00$ and 0.10 , respectively.^{8,19} Both the pure and Ir-substituted samples exhibit metallic behavior in the normal state, and the value of $d\rho/dT$ is higher in Ir-doped compounds. Subtle falls in the $\rho(T)$ curves near 130 K correlate well in temperature with the onset of magnetic ordering, and are probably related to the suppression of the spin-flip scattering. This feature is clearly observed as a maximum in the $d\rho/dT$ data near the magnetic ordering temperature $T_M \sim 130\text{ K}$ for $x = 0.00$, as shown in the inset of Fig. 2. Below T_M , the $\rho(T)$ curves of Ru(Ir)-1212 specimens exhibits an extended metallic region, which is consistent with a simple two-band model proposed recently.²⁰ The electrical resistivity displays a shallow minimum near 65 K for the sample with $x = 0.00$, and a more pronounced one at 72 K for the compound with $x = 0.10$. The $\rho(T)$ minimum is followed by a slight upturn in $\rho(T)$ close to the onset of the superconductivity ($T_{c,onset}$). This upturn is hardly seen in samples with low Ir content; however it becomes discernible in the specimen with $x = 0.10$. In addition, the $T_{c,onset}$ decreases from $\sim 50\text{ K}$ for $x = 0.00$ to $\sim 30\text{ K}$ for $x = 0.10$.

These features may be related to the electronic mean free path which can be extracted from the ρ according to²¹

$$l = \frac{(4.95 \times 10^{-4})v_F}{(\hbar w_p)^2 \rho}, \quad (1)$$

where v_F is the Fermi velocity, assumed to be $2.5 \times 10^{-7}\text{ cm/s}$, and ρ is given in $\mu\Omega\text{cm}$.^{22,23} Considering $\hbar w_p \sim 0.2\text{ eV}$,²¹ the values of l at 300 K were calculated using Eq.(1) and are

summarized in Table II. For the sample with $x = 0.00$, $l = 21 \text{ \AA}$ a value that decreases with increasing Ir concentration, reaching $l = 15 \text{ \AA}$ for the $x = 0.10$ composition. For the Ru-1212 compound, l is over 10 times larger than the typical Cu-O bond length ($\sim 1.9 \text{ \AA}$) in these materials. In addition, this value is lower than that observed for Ru-1222 (close to 58 \AA)²⁴ but comparable to the ones found in other high- T_c cuprates.²¹ One can also infer from the $\rho(T)$ data that increasing Ir content results in a systematic decrease of the superconducting transition temperature and an increase of the normal-state electrical resistivity. These features may have their counterpart in the magnetic properties of these Ru(Ir)-1212 compounds, as discussed below.

The ZFC (open symbols) and FC (full symbols) measurements of magnetization in Fig.3 were taken in the remnant field of the superconducting magnet ($H \sim 1 \text{ Oe}$) for samples with Ir content $x = 0, 0.05$, and 0.10 . At temperatures below 30 K , these compounds exhibit superconductivity and diamagnetic contributions are clearly observed in both ZFC and FC curves. On the other hand, no diamagnetic signature has been observed for $M(T)$ measurements in very low applied magnetic fields, as low as $H = 5 \text{ Oe}$ (data not shown). The absence of appreciable diamagnetism in low applied fields is a common feature of these Ru-1212 compounds. The strength of the diamagnetic response is strongly dependent on sample preparation and, consequently, on the relative volume fraction of superconducting and non-superconducting phases due to the so-called spontaneous vortex phase, which arises even in zero applied magnetic field.⁵ For temperatures below 15 K , a positive upturn in the FC magnetization curve associated with the paramagnetic contribution of the Gd^{3+} ions has been observed. Such a feature is in excellent agreement with heat capacity measurements (data not shown) that suggest the development of antiferromagnetic ordering below $T \sim 2.5 \text{ K}$ at the Gd sublattice for samples with $x = 0.00$ and $x = 0.10$. However, we have observed that the Neel temperature of the Gd sublattice is not modified by the Ir substitution. This further indicates that Ir preferentially substitutes Ru in this series.

In the upper inset of Fig. 3, the magnetic ordering transition of the Ru-sublattice is inferred from a pronounced peak in the in-phase component of the $\chi_{ac}(T)$ magnetic susceptibility data. A careful inspection of the figure indicates that $\chi_{ac}(T_M) = 130 \text{ K}$ for the sample with $x = 0.00$. The magnetic transition temperature T_M is very sensitive to the Ir concentration and decreases to $T_M \sim 112 \text{ K}$ for the sample with $x = 0.10$. Also, from the upper inset of Fig. 3, one is able to infer that the magnitude of the magnetic moment

decreases with increasing Ir concentration. The latter result, combined with the gradual decrease of T_M with increasing Ir content, is compelling evidence that Ir does replace Ru in this series. In the lower inset of Fig. 3, T_M as a function of Ir content is displayed. The results indicate that T_M decreases linearly with Ir content at the rate of ~ -1.6 K/Ir at %. Values of T_M are summarized in Table II.

The suppression of the diamagnetic signal in Ru(Ir)-1212 at very low applied magnetic fields ~ 5 Oe is of interest and has been discussed previously for similar compounds.⁹ It was argued that these oxides are comprised of two different phases due to a phase separation phenomenon: one superconducting and another one which is magnetic. These phases, which are believed to exist in a nanoscale dimensions, are homogeneously distributed throughout the material and coexist at low temperatures, a morphology similar to granular superconductors.²⁵ Within this context, the absence of appreciable diamagnetism is a consequence of the reduced dimensions of the superconducting regions which are comparable to the large London penetration depth, as discussed elsewhere.²⁵ Thus, in order to clarify the effects caused by the application of applied magnetic fields on the superconducting properties of Ir-substituted Ru-1212 materials we have carried out magnetoresistivity $\rho(H, T)$ measurements in applied magnetic fields up to 18 T. Few selected curves of $\rho(H, T)$ are shown in Fig. 4 for two samples with $x = 0.00$ and 0.10. The $\rho(H, T)$ curves for the sample with $x = 0.00$ indicate that $T_{c,onset}$ remains nearly constant ~ 50 K under magnetic fields. On the other hand, the temperature in which zero-resistance is attained ($T_{c,zero}$) decreases rapidly for low applied magnetic fields ($H \leq 2$ T), followed by a much less pronounced drop in higher H . These features certainly resemble the ones observed in granular superconductors.²⁵ We mention that the $\rho(T, H = 0)$ curves displayed in Fig. 4 were taken in the remnant field of the Nb₃Sn superconducting magnet, estimated to be ~ 0.03 T. Therefore, the transition width of $\rho(T)$ is broadened from the expected one for the true zero-field data. The $\rho(H, T)$ data also show that the sample with the lowest $T_{c,onset}$ ($x = 0.10$) attains the zero-resistance state at $T \geq 2$ K even for the highest applied magnetic field of 18 T. This result reinforces the picture of a granular behavior in this series since pathways are still preserved within the material even at 18 T. A detailed analysis of the low-field data probing the granular properties of these materials is described below.

In order to further probe the effect of the applied magnetic field on the resistive transition, the derivative curves of the electrical resistance versus temperature were constructed. For

example, displayed in Fig. 5 are the $d\rho(H,T)/dT$ curves for the Ir-doped sample with $x = 0.02$ taken at several applied magnetic fields. At $H = 0$, a sharp peak at $T_1 \sim 38$ K is observed. The value of T_1 depends on the concentration of Ir; for $H = 0$, the transition temperature decreases from $T_1 \sim 39$ K ($x = 0.00$) to $T_1 \sim 22$ K ($x = 0.10$). The value of T_1 is nearly magnetic field independent H up to 0.5 T. However, two features in the $H \sim 0.035 - 0.500$ range are of interest: (i) the reduction in the peak intensity; and (ii) a pronounced broadening of the peaks, culminating in a split into two convoluted peaks. A further increase in $H \geq 0.5$ T results in a progressive reduction of the amplitude of the high temperature peak, leading to its gradual suppression, and the appearance of another peak at low temperatures for applied magnetic fields $H \sim 1 - 2$ T. The amplitude of the peak at lower temperatures increases strongly with H , and its position is monotonically shifted towards lower temperatures. Similar double-peak structure and its evolution with H were observed for all samples studied. However, the $d\rho(H,T)/dT$ curves at high magnetic fields ($H \geq 2$ T) reveal that the amplitude, width, and position of the lower peak depend on the Ir content (see inset of Fig. 5). For $H = 14$ T, the intensity of the peak increases and its width decreases with increasing Ir concentration.

We also mention that similar magnetic field dependence of the double peak behavior seen in $d\rho(H,T)/dT$ curves has been previously observed in both Ru-1212 and Ru-1222 compounds.^{24,25,26} The two-peak feature in $d\rho(H,T)/dT$ versus T data is usually related to the development of superconductivity within the grains (intragrain) and between grains (intergrain) at an upper and lower temperatures, respectively.²⁵ However, it has been argued that ruthenocuprates exhibit granular behavior, a feature consistent with a phase separation of mesoscopic superconducting and non-superconducting phases even within the grains.^{9,10} In the present case one may consider that Ru ions are replaced by Ir and this would affect preferably the intragrain properties, as inferred from both $M(T)$ and $\rho(T)$ data. On the other hand, the inset on Fig. 5 shows that Ir substitution changes the shape of the low temperature peak in $d\rho(H,T)/dT$ at high applied H . Such an observation suggests that the low temperature peak at high H may not be related only to the so-called intergranular transition. In fact, as the studied samples attain zero resistance state at $T \geq 2$ K up to highest applied magnetic fields of 18 T, it is expected that the intragrain transition takes place at magnetic fields within the studied range. Our results evidence a strong-field dependence on both the magnetic and transport properties of the Ru(Ir)-1212, indicating

that inhomogeneities are present within physical grains.

Such a double-peak structure in $d\rho(H,T)/dT$ versus T in ruthenocuprates has been previously observed and discussed within the scenario of with weakly disordered Josephson-junction arrays (JJA).^{9,10} It was argued that nanoscale superconducting domains are coupled through Josephson junctions below the thermodynamic transition temperature, as a consequence of a phase separation into FM and AFI regions.^{9,10} Our results seem to be consistent with such a scenario also due to the fact that the high temperature peak vanishes for applied magnetic fields $H \sim 1 - 2$ T, which is actually the same value where a spin flop-like transition has been observed.⁴ Thus, it seems reasonable to consider that even though granular behavior may be present, the magnetoresistivity results of the Ir-substituted samples suggest that the lower and high temperature peaks are a consequence of the intragrain granular structure due to a phase separation.

The main effect of the applied magnetic field is the broadening of the resistive transition due to the movement of vortices (see Figs. 4 and 5). This result indicates the presence of dissipation phenomena as commonly observed in conventional high-temperature superconductors. Thus, by using the Arrhenius-type expression²⁷

$$\rho = \rho_0 e^{-\frac{U}{k_B T}}, \quad (2)$$

where ρ_0 is the order of $\rho(300$ K) and k_B is the Boltzmann constant, one is able to fit the low part of $\rho(H, T)$ curves to obtain the vortex thermal activation energy U . Fig. 6 shows the Arrhenius plots of the resistive transitions for the sample with $x = 0.05$ in applied magnetic fields up to 18 T. Pinning energies U can be estimated from the slopes, over which the data can be represented by a straight line, as shown by solid lines in Fig 6. The same procedure has been adopted for other samples and the U values obtained for the $x = 0.05$ sample, when the applied field increases from 0 to 18 T, are $U = 60$ meV and 5 meV, respectively. The inset of Fig. 6 shows the U values for $x = 0.00$ and $x = 0.05$ as a function of the applied magnetic field. At $H = 0.005$ T, as the Ir content increase from $x = 0.00$ to $x = 0.05$, the U value decreases from 100 meV to 60 meV probably due to the narrowing of the superconducting transition with increasing Ir content. For higher applied fields, U decreases and assumes a nearly constant value, roughly in the range 3 - 5 meV. The magnetic field dependence of U and their saturation values are similar to those found in Ru-1212 compound²⁸ and $\text{Bi}_2\text{Sr}_2\text{CaCu}_2\text{O}_8$ (BSCCO-2212) system.²⁹ However, it is important

to notice that values of U in the range 5 - 30 meV are much lower than the ones found for the less anisotropic compound YBCO which is close to 100 meV.³⁰

From the inset of Fig. 6, one observes that the magnetic field dependence of the activation energy U can be described by a power-law behavior that can be written as $U \sim H^{-\beta}$. From the fitting parameters we have estimated $\beta \sim 0.33$ and 0.32 for $x = 0.00$ and $x = 0.05$, respectively. Values of β are of interest because they reflect the dimensionality of the vortex lattice.³¹ For instance, values of β comprehended between 0.33 - 0.5, as found in the BSCCO-2212 system, indicate a two-dimensional character of the vortex lattice.^{29,30} On the other hand, $\beta \sim 1$, as usually found in YBCO cuprates, suggests a three-dimensional character of the vortice lattice.³² Thus, our data strongly indicate that both Ru-1212 and Ir-doped Ru-1212 compounds are very anisotropic and can be classified as having a vortex lattice with two-dimension character.

The magnetoresistivity data are also useful for an estimate of the temperature dependence of the upper critical field $H_{c2}(T)$ in this series. The temperature dependence of $H_{c2}(T)$ of Ru(Ir)-1212 compounds is displayed in Fig. 7, along with the data for the Ru-1222 compound for comparison.²⁴ The phase diagram was determined by using the $\rho(H,T)$ curves, considering the same $T_{c,onset}$ for all applied magnetic fields and by taking a 50 % drop of $\rho(T)$ as the criterium for the determination of H_{c2} . The Ru(Ir)-1212 curves display essentially the same trend and H_{c2} shifts to lower temperatures with increasing Ir content. At high applied magnetic fields, the upper-critical-field phase diagram shows a linear increase of H_{c2} with slopes -3.2 T/K for $x = 0.00$ and -10 T/K for $x = 0.10$. On the other hand, by using the phenomenological relation

$$H_{c2}(T) = H_{c2}(0) \left[1 - \left(\frac{T}{T_c} \right)^2 \right]^\alpha, \quad (3)$$

one can obtain an estimate of $H_{c2}(0)$ and α . The best fitting procedures using Eq. 3 for the data are plotted in dashed lines in Fig. 7. Fixing the same T_c used before, the calculated parameters were $H_{c2}(0) \sim 52$ T and $\alpha \sim 1.8$ for the sample with $x = 0.00$. The values obtained for all samples are summarized in Table II. Values of α in the 1.5 - 2.0 range are frequently observed and are in line with the reported values for other high- T_c materials.³³ However, we mention that values of $H_{c2}(0)$ for pure and doped compounds are higher than the ones found for Ru-1222. In addition to this, increasing Ir content has little effect in the

values of $H_{c2}(0)$.

From previous studies and by considering the values obtained for the pinning energy it is possible to infer that the highly anisotropic behavior of Ru-1212 compounds is similar to the BSCCO-2212 superconductor. The anisotropy factor $\gamma = H_{c2}^{ab}/H_{c2}^c$ of BSCCO-2212 compounds has been estimated to be in the range between 50 and 200.³¹ By considering a similar anisotropy to Ru-1212 compounds, the estimated value of H_{c2} would reflect the upper critical field parallel to the a - b plane, and the superconducting coherence length $\xi_c(T)$ can be estimated. This can be done by assuming that $H_{c2}(T) \simeq H_{c2}^{ab}(T) = \Phi_0/2\pi\xi_c^2(T)$, where Φ is the magnetic flux quantum. The estimated values of $\xi_c(0) \sim 24 \text{ \AA}$ are shown in Table II. They indicate that all the samples studied have similar values of $\xi_c(0)$, i.e., that Ir-substitution has little effect on the coherence length in this series. These results suggest that the partial substitution of Ru by Ir changes the character of the Ru-O planes and acts on the coupling between planes. This is reflected in the nearly constant H_{c2} for all the series even when T_c is drastically reduced. Such an increasing coupling between Cu planes can be also inferred from the progressive narrowing of the superconducting transition, as shown in Fig. 4.

SUMMARY

The magnetic and transport properties of $\text{Ru}_{1-x}\text{Ir}_x\text{Sr}_2\text{GdCu}_2\text{O}_8$; $0 \leq x \leq 0.10$; compounds were investigated. The main results indicate that Ir substitutes Ru ions with no significant structural distortions due to similar ionic radii. The substituted Ir dilutes the Ru magnetic sub-lattice, decreasing both the magnetic ordering and the superconducting transition temperatures. The magnetoresistivity data revealed that all samples are superconducting up to 18 T at temperatures higher than 2 K. On the other hand the diamagnetic signal in the magnetization curves is absent for low applied magnetic field. The combined results indicate that the ruthenocuprates have similar anisotropic properties as observed in bismuth based high-temperature superconductors. In addition, the Ir substitutions and the effect of the applied magnetic field on the electrical resistance curves suggest that the granular behavior observed may be related to phase separation of ferromagnetic and anti-ferromagnetic mesoscopic regions.

Acknowledgments

This work was supported by the Brazilian Agency FAPESP under Grant Nos. 05/53241-9, 01/01455-4, and 01/04231-0, and by the US National Science Foundation under Grant No. DMR-0306165 (MST). Work at the NHMFL was performed under the auspices of the NSF, the State of Florida, and the U.S. Department of Energy. A. R. Jurelo, F. C. Fonseca, and R. F. Jardim are CNPq fellows under Grant Nos. 150845/2004-9, 301661/2004-9, and 303272/2004-0, respectively.

* Permanent address: Universidade Estadual de Ponta Grossa, Ponta Grossa, Paraná, Brazil.

† Electronic address: rjardim@if.usp.br

References

- ¹ L. Bauernfeind, W. Widder, and H. F. Braun, *Physica C* **254** (1995) 151.
- ² C. Bernhard, J. L. Tallon, Ch. Niedermayer, Th. Blasius, A. Golnik, E. Brucher, R. K. Kremer, D. R. Noakes, C. E. Stronach, and E. J. Ansaldo, *Phys. Rev. B* **59** (1999) 14099.
- ³ I. Felner, E. Galstyan, R. H. Herber, and I. Nowik, *Phys. Rev. B* **70** (2004) 94504.
- ⁴ G. V. M. Williams and S. Krämer, *Phys. Rev. B* **62** (2000) 4132.
- ⁵ E. B. Sonin and I. Felner, *Phys. Rev. B* **57** (1998) 14000.
- ⁶ H. S. Greenside, E. I. Blount, and C. M. Varma, *Phys. Rev. Lett.* **46** (1981) 49.
- ⁷ I. Felner, U. Asaf, Y. Levi, and O. Millo, *Phys. Rev. B* **55** (1997) R3374.
- ⁸ A. C. McLaughlin, W. Zhou, J. P. Attfield, A. N. Fitch, and J. L. Tallon, *Phys. Rev. B* **60** (1999) 7512.
- ⁹ B. Lorenz, Y. Y. Xue, R. L. Meng, and C. W. Chu, *Phys. Rev. B* **65** (2002) 174503; Y. Y. Xue, B. Lorenz, A. Bailakov, D. H. Cao, Z. G. Li, and C. W. Chu, *Phys. Rev. B* **66** (2002) 014503.
- ¹⁰ *Ruthenate and Rutheno-Cuprate Materials*, edited by C. Noce, A. Vecchione, M. Cuoco, and A. Romano (Springer, Germany, 2002).
- ¹¹ A. C. McLaughlin, and J. P. Attfield, *Phys. Rev. B* **60** (1999) 14605.
- ¹² A. Hassen, J. Hemberger, A. Loidl, and A. Krimmel, *Physica C* **400** (2003) 71.
- ¹³ G. V. M. Williams, Ho Keun Lee, and S. Krämer, *Phys. Rev. B* **67** (2003) 104514.
- ¹⁴ Z. Sun, S. Y. Li, Y. M. Xiong, and X. H. Chen, *Physica C* **349** (2001) 289.
- ¹⁵ See, for instance, T. P. Papageorgiou, T. Herrmannsdorfer, R. Dinnebier, T. Mai, T. Ernst, M. Wunschel, and H. F. Braun, *Physica C* **377** (2002) 383; R. F. Jardim, E. A. Early, and M. B. Maple, *J. Alloys Comp.* **221** (1995) 1.
- ¹⁶ S. Andrade, F. C. Fonseca, R. F. Jardim, I. Bossi, M. S. Torikachvili, A. H. Lacerda, and L. Ben-Dor, *Braz. J. Phys.* **33** (2003) 686.
- ¹⁷ R. D. Shannon, *Acta Cryst. A* **32** (1976) 751.
- ¹⁸ A. J. Dos Santos-Garcia, M. H. Aguirre, E. Moran, R. Saez Puche, and M. A. Alario-Franco, J.

- Solid State Chem. **179** (2006) 1296.
- ¹⁹ Z. Sun, S. Y. Li, Y. M. Xiong, and X. H. Chen, *Physica C* **349** (2001) 289.
- ²⁰ J. E. McCrone, J. L. Tallon, J. R. Cooper, A. C. MacLaughlin, J. P. Attfield, and C. Bernhard, *Phys. Rev. B* **68** (2003) 64514.
- ²¹ M. Gurvitch, and A. T. Fiory, *Phys. Rev. Lett.* **59** (1987) 1337.
- ²² J. Mesot, M. R. Norman, H. Ding, M. Randeria, J. C. Campuzano, A. Paramakanti, H. M. Fretwell, A. Kaminski, T. Takeuchi, T. Yokoya, T. Sato, T. Takahashi, T. Mochiku, and K. Kadowaki, *Phys. Rev. Lett.* **83** (1999) 840.
- ²³ M. Chiao, R. W. Hill, C. Lupien, L. Taillefer, P. Lambert, R. Gagnon, and P. Fournier, *Phys. Rev. B* **62** (2000) 3354.
- ²⁴ M. T. Escote, V. A. Meza, R. F. Jardim, L. Ben-Dor, M. S. Torikachvili, and A. H. Lacerda, *Phys. Rev. B* **66** (2002) 144503.
- ²⁵ R. F. Jardim, M. C. de Andrade, E. A. Early, M. B. Maple, and D. Stroud, *Physica C* **232** (1994) 145.
- ²⁶ S. Garcia, J. E. Musa, R. S. Freitas, and L. Ghivelder, *Phys. Rev. B* **68** (2003) 144512.
- ²⁷ P. W. Anderson and Y. B. Kim, *Rev. Mod. Phys.* **38** (1975) 1049.
- ²⁸ C. Attanasio, M. Salvato, R. Ciancio, M. Gombos, S. Pace, S. Uthayakumar, and A. Vecchione, *Physica C* **411** (2004) 126. X. H. Chen, Z. Sun, K. Q. Wang, S. Y. Li, Y. M. Xiong, M. Yu, and L. Z. Cao, *Phys. Rev B* **63** (2001) 64506.
- ²⁹ C. Attanasio, C. Coccorese, V. N. Kushnir, L. Maritato, S. L. Prischepa, and M. Salvato, *Physica C* **255** (1995) 239.
- ³⁰ T. T. M. Palstra, B. Batlogg, R. B. van Dover, L. F. Schneemeyer, and J. V. Waszczak, *Phys. Rev. B* **41** (1990) 6621.
- ³¹ G. Blatter, M. V. Feigel'man, V. G. Geshkenbein, A. I. Larkin, and V. M. Vinokur, *Rev. Mod. Phys.* **66** (1994) 1125.
- ³² T. T. M. Pastra, B. Batlogg, R. B. van Dover, L. F. Schneemeyer, and J. V. Waszczak, *Appl. Phys. Lett.* **54** (1989) 763.
- ³³ *Introduction to Superconductivity and High-TC Materials*, edited by M. Cyrot and D. Pavuna (World Scientific, Singapore, 1992).

Figure Captions

Figure 1: XRD patterns taken at room temperature of polycrystalline samples of $\text{Ru}_{1-x}\text{Ir}_x\text{Sr}_2\text{GdCu}_2\text{O}_8$; $x = 0.00$ and 0.10 . The figure displays the experimental data (dots), the calculated diffraction pattern (solid lines), and the difference between them. The arrow points to the removed 2Θ region where the main diffraction peaks of the $\text{Sr}_2\text{GdRuO}_6$ and SrRuO_3 extra phases appear. The inset exhibits the calculated lattice parameters (a and c) as a function of the Ir content.

Figure 2: Temperature dependence of the electrical resistivity in zero external magnetic field of $\text{Ru}_{1-x}\text{Ir}_x\text{Sr}_2\text{GdCu}_2\text{O}_8$ for Ir concentrations $x = 0.00, 0.02, 0.05,$ and 0.10 . The inset displays $d\rho/dT$ versus temperature for the compound with $x = 0.00$ in the neighborhood of T_M .

Figure 3: ZFC (open symbols) and FC (full symbols) magnetization curves as a function of the temperature for $\text{Ru}_{1-x}\text{Ir}_x\text{Sr}_2\text{GdCu}_2\text{O}_8$; $0 \leq x \leq 0.10$; measured under the remnant field of the magnet ($H \sim 1$ Oe). Upper inset: temperature dependence of the in-phase component of the $\chi_{ac}(T)$ near the magnetic ordering temperature T_M . Lower inset: plot of the T_M as a function of the Ir content.

Figure 4: Electrical resistivity versus temperature at several applied magnetic fields to 18 T for the $\text{Ru}_{1-x}\text{Ir}_x\text{Sr}_2\text{GdCu}_2\text{O}_8$; $x = 0.00$ and $x = 0.10$; compounds. The remnant field of the superconducting magnet has been estimated to be 0.03 T.

Figure 5: Temperature dependence of the derivative of the electrical resistivity for the compound $\text{Ru}_{0.98}\text{Ir}_{0.02}\text{Sr}_2\text{GdCu}_2\text{O}_8$ in applied magnetic fields up to 18 T. The upper inset displays a plot of $d\rho/dT$ versus temperature at $H = 14$ T in samples with Ir concentrations $x = 0.00, x = 0.05,$ and $x = 0.10$.

Figure 6: Arrhenius plot of the electrical resistivity data for the compound $\text{Ru}_{0.95}\text{Ir}_{0.05}\text{Sr}_2\text{GdCu}_2\text{O}_8$. The solid lines represent the best fit to the data by using Eq. (2). The inset displays a plot of thermal activation energy versus applied magnetic

field for the sample with $x = 0.00$ (open symbols) and $x = 0.05$ (full symbols).

Figure 7: Temperature dependence of the upper critical field of Ru-1212, Ir-doped Ru-1212, and Ru-1222. The dashed lines correspond to the fitting of Eq. 3. The high-field slope dH_{c2}/dT is shown in solid lines.

TABLE I: Unit cell parameters, atomic parameters, and agreement factors for $\text{Ru}_{1-x}\text{Ir}_x\text{Sr}_2\text{GdCu}_2\text{O}_8$; $x = 0.00$ and $x = 0.10$; obtained through Rietveld refinements at room temperature. The space group is $P4/mmm$. The occupancy and the thermal factors were fixed according to the results of Ref. [8].

	$a = b$ (Å)	c (Å)	V (Å ³)	R_{wp}	R_p	χ^2
$x = 0.00$	3.8389(4)	11.5652(2)	170.44(3)	0.0466	0.0367	1.57
$x = 0.10$	3.8399(1)	11.5644(5)	170.51(2)	0.0578	0.0458	2.12
Atom	Site	x	y	z	U	Occupancy
Ru	1b	0	0	0.5	0.0001	1(0.9)
(Ir)		0	0	0.5		(0.1)
Sr	2h	0.5	0.5	0.3137(3)	0.0001	1
				0.3137(4)		
Gd	1c	0.5	0.5	0	0.0001	1
Cu	2g	0	0	0.1437(4)	0.0001	1
				0.1461(6)		
O(1)	8s	0.008	0	0.330	0.008	0.5
		0.007		0.334		
O(2)	4i	0	0.5	0.125(1)	0.008	1
				0.122(2)		
O(3)	4O	0.138(5)	0.5	0.5	0.008	0.25
		0.158(7)				

TABLE II: Several physical parameters extracted from magnetic and transport properties of $\text{Ru}_{1-x}\text{Ir}_x\text{Sr}_2\text{GdCu}_2\text{O}_8$; $0 \leq x \leq 0.10$. The parameters are described in the text and the corresponding ones belonging to the Ru-1222 compound are also displayed for comparison.²⁴ The value of T_c has been obtained by taking the 50 % drop of $\rho(T)$ and both $H_{c2}(0)$ and α from a phenomenological equation by considering T_c fixed.

Ir	$T_c(\text{K})$	$l(\text{\AA})$	$H_{c2}(0)$	α	$\xi_c(\text{\AA})$	$T_M(\text{K})$
0.00	39	21	52	1.8	25	130
0.02	38	21	53	1.7	24	126
0.05	32.5	15	53	2.0	24	120
0.10	22	15	54	2.8	24	112
Ru-1222	39	58	39	1.8	28	100

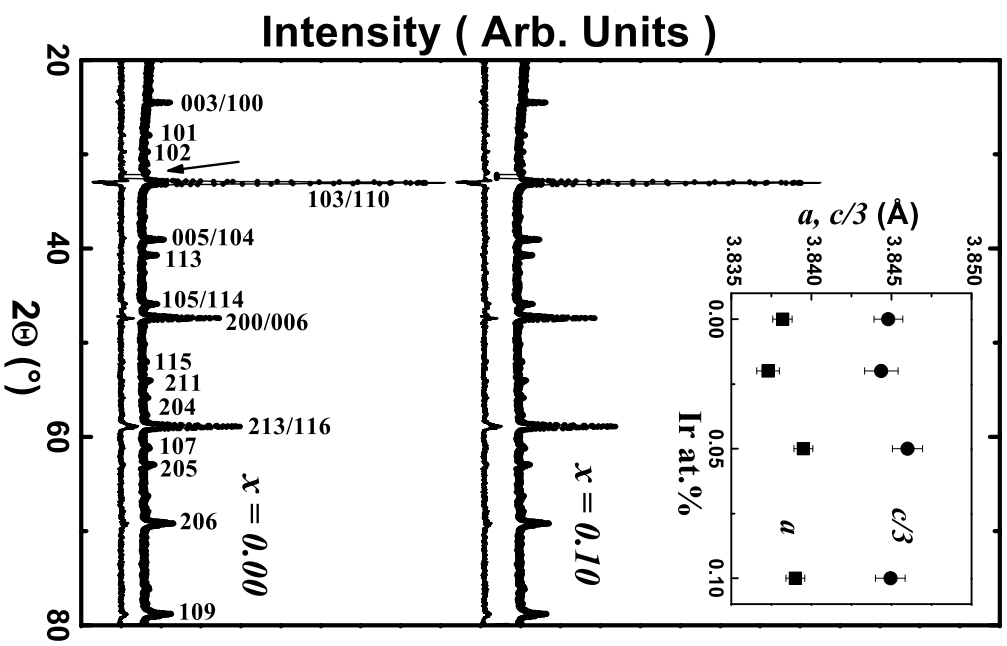


FIG. 1: A. R. Jurelo et al.

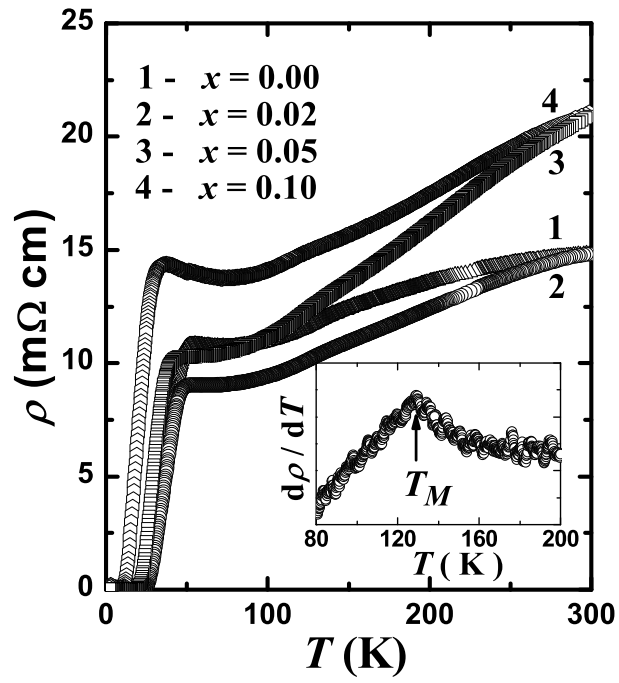


FIG. 2: A. R. Jurelo et al.

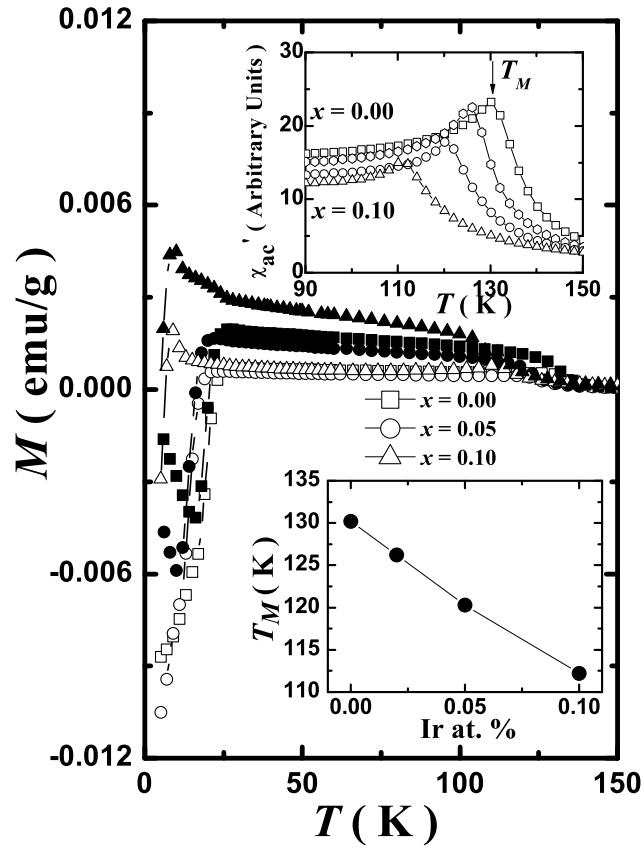


FIG. 3: A. R. Jurelo et al.

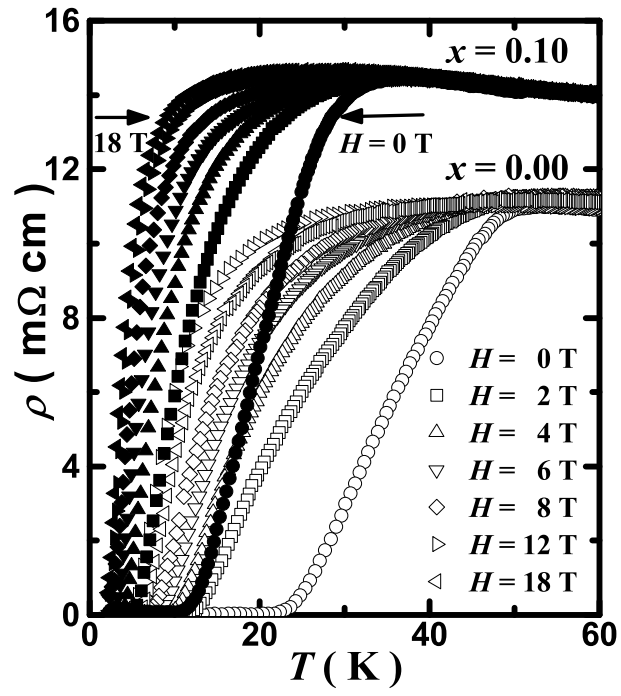


FIG. 4: A. R. Jurelo et al.

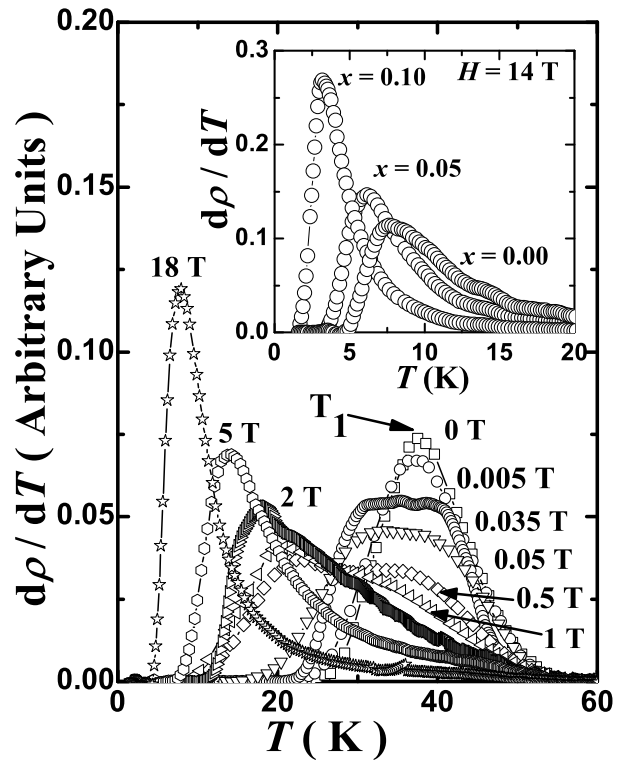


FIG. 5: A. R. Jurelo et al.

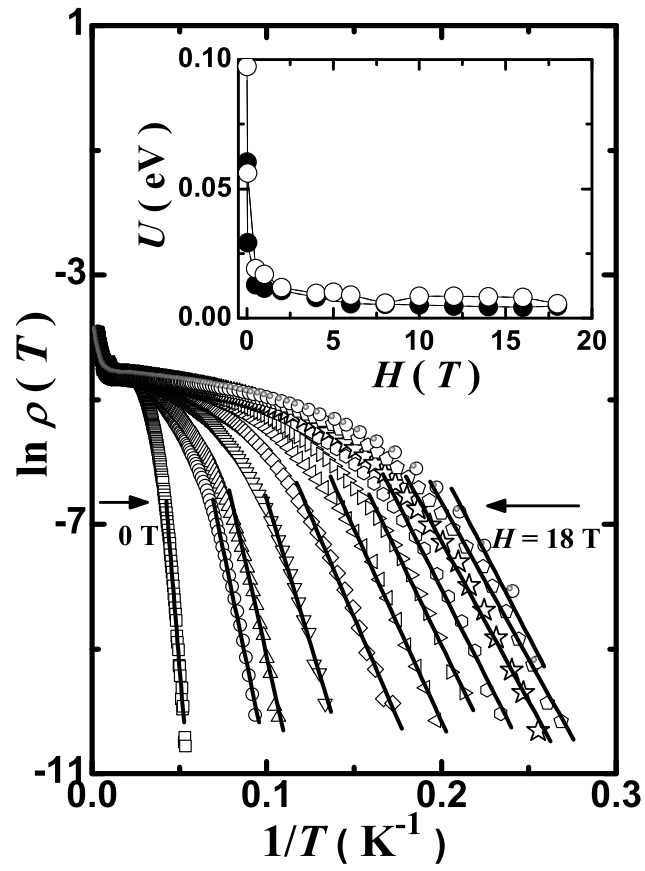


FIG. 6: A. R. Jurelo et al.

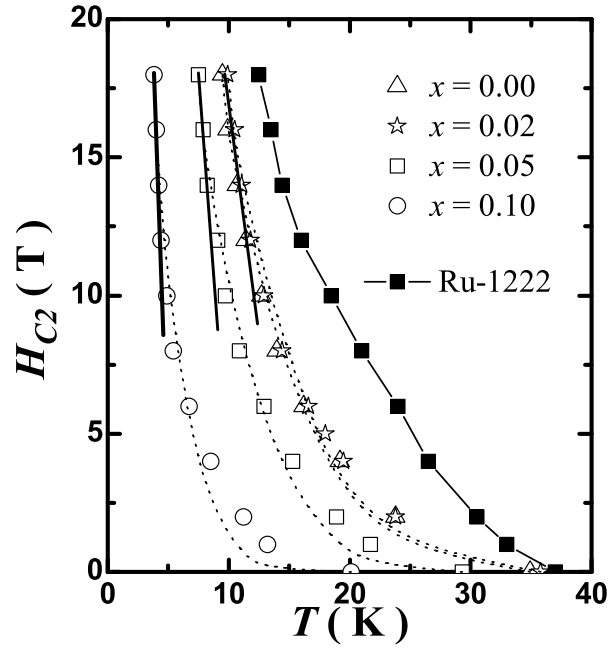


FIG. 7: A. R. Jurelo et al.